

Coordinated Stress-Structure Self-Organization in Granular Packing

Xiaoyu Jiang* and Takashi Matsushima†
*Department of Engineering Mechanics and Energy,
 University of Tsukuba, Tsukuba, Ibaraki, 305-8573, Japan*

Raphael Blumenfeld‡
*Gonville & Caius College, University of Cambridge, UK
 (Dated: August 16, 2022)*

It is accepted that stress and structure self-organize cooperatively during quasi-static dynamics of granular systems, but the consequences of this self-organization are not fully understood. Such an understanding is essential because local structural properties of the settled material are then correlated with the local stress, which calls into question existing linear theories of stress transmission in granular media. A method to quantify the local stress-structure correlations is necessary for addressing this issue and we present here such a method for planar systems. We then use it to analyze numerically several different systems, compressed quasi-statically by two different procedures. We define cells, cell orders, cell orientations, and cell stresses and report the following. 1. The mean ratio of cell principal stresses decreases with cell order and increases with friction. 2. The ratio distributions collapse onto a single curve under a simple scaling, for all packing protocols and friction coefficients. 3. Cells orient along the local stress major principal axes. 4. A simple first-principles model explains the correlations between the local cell and stress principal axis orientations. Our results quantify the cooperative stress-structure self-organization and provide a way to relate quantitatively the stress-structure coupling to different process parameters and particle characteristics. Significantly, the strong stress-structure correlation, driven by structural re-organization upon application of external stress, suggests that current stress theories of granular matter need to be revisited.

Granular matter plays an important role in nature and in our everyday life, but understanding its rich and complex behavior is far from complete. One difficulty is that the sensitivity of macroscopic behavior to grain-scale structural characteristics hinders conventional coarse-graining methods. A fundamental difficulty is that theories for mechanics of such media are often based on the assumption that the macroscopic constitutive properties can be taken as independent of the stress. This assumption makes possible explicit solutions for the stress field, but there is a growing realization [1–4] that the local structure and stress self-organize cooperatively and preliminary observations were made on the stress-structure coupling [5]. Such a coupling undermines the assumption of independence of local constitutive properties because any applied stress causes a correlated re-organisation of the local structure and suggests that the stress field equations *cannot be linear*. While much effort focused on the relations [6] between deformation of granular materials and force chains [7] on the grain-scale structure [1, 8–10], characterizing the effects of the stress-structure co-organization has been elusive. Here we uncover and quantify these effects in a range of planar systems.

In two dimensions, mechanically stable structures can be described in terms of cells, which are the smallest voids surrounded by particles in contact, as illustrated in Fig. 1. The cell dynamics have proved useful to quantify kinetic processes [11, 12], and to study organization of structural characteristics and

entropic effects [4, 13–15]. By simulating a range of differently compressed planar systems, we study the self-organization of cells and the stress field. We define cell stresses and find that: 1. under simple scaling, the distributions of cell stress ratios of all the systems collapse onto one Weibull curve; 2. cells orient along the directions of the local principal stresses. We identify the effects of friction and cell order on these phenomena. Finally, we introduce a simple model that explains the stress-structure orientation correlations. Our results establish and quantify the stress-structure coupled self-organization. They also show that a cell-based description is essential to the understanding of the structural evolution of granular materials. This study further suggests that current linear models of stress transmission in granular material may need to be modified.

Numerical simulations

The numerical simulations were carried out using the Discrete Element Method (DEM) [16]. The initial state was generated by placing $N = 50,000$ discs randomly within a double periodic domain. The discs' radii, r , were distributed uniformly between 0.667 and 1.333, with a mean $\bar{r} = 1$. The initial packing fraction was set to below jamming, $\phi = 0.7$, making the initial system dimensions $L_x = L_y \approx 282.5\bar{r}$. The disc peripheries were assigned a friction coefficient μ and the system was slowly compressed by two different protocols: isotropic (ISO) and anisotropic (ANISO). We

\bar{z}	$\mu = 0.01$	0.1	0.2	0.5	1.0	10.0
ISO	3.98	3.70	3.51	3.21	3.11	3.07
ANISO	3.98	3.70	3.51	3.21	3.11	3.07

$\langle \delta^2 z \rangle$	$\mu = 0.01$	0.1	0.2	0.5	1.0	10.0
ISO	0.85	0.83	0.83	0.84	0.84	0.82
ANISO	0.86	0.82	0.83	0.84	0.83	0.82

TABLE I. The systems' mean coordination numbers, \bar{z} , and standard deviations, $\langle \delta^2 z \rangle$.

studied twelve systems, with each protocol applied with $\mu = 0.01, 0.1, 0.2, 0.5, 1.0$, and 10 . Systems were compressed by changing the periodic length in two directions in ISO and one direction in ANISO. During a compression step, disc center positions, (x_i, y_i) , were shifted using

$$\alpha_i(t + \Delta t) = \frac{L_\alpha(t + \Delta t)}{L_\alpha(t)} \alpha_i(t) \quad ; \quad \alpha_i = x_i, y_i. \quad (1)$$

This ensured a uniform strain across the system. The system's stress state is

$$\Sigma_{\alpha\beta} = \frac{1}{L_x L_y} \sum_{i < j} f_{\alpha}^{ij} l_{\beta}^{ij}, \quad (2)$$

where f_{α}^{ij} is the α -component of the contact force between discs i and j and l_{β}^{ij} is the β -component of the position vector pointing from disc j 's center to that of disc i . Compression continued until two conditions were met: (i) the system reached a jammed mechanically stable state, in which the kinetic energy fell below a very small magnitude $E_k < 10^{-17} k_n \bar{r}^2$ per disc, where k_n is the spring stiffness of our contact model ($= 10^7 \text{N/m}$ in our simulations); (ii) the system stresses, $\Sigma_{xx} = \Sigma_{yy}$ in ISO and Σ_{yy} in ANISO, reached a threshold value $\Sigma_c = k_n \bar{\delta} = 10^2$, with $\bar{\delta}$ the average overlap between discs (limited to $10^{-5} \bar{r}$ to approximate disc rigidity).

We then generated the coordination number histograms in each system, ignoring rattlers, and calculated the means, \bar{z} , and standard deviations, $\langle \delta^2 z \rangle$. These we summarize in Table I. The values of \bar{z} ranged from 3.98 for $\mu = 0.01$ to 3.07 for $\mu = 10.0$ in both ISO and ANISO systems, showing that all the systems were very close to being marginally rigid. For the ANISO processes, we also measured the stress ratios Σ_{xx}/Σ_{yy} and found that these decreased from 0.948 for $\mu = 0.01$ to 0.815 for $\mu = 10.0$.

Relations between cell order and stress

Our analysis of the generated packings is cell-based [9] (see Fig. 1). Defining a cell center as the mean position of the contact points around it, we proceed to define a cell stress σ^c through the stresses of the discs surround-

ing it. Let the stress of disc g be

$$\sigma^g = \frac{1}{A^g} \sum_{g'} l^{gg'} \otimes f^{g'g}, \quad (3)$$

where g' are the discs in contact with g , $l^{gg'}$ the position vector pointing from the center of g to the contact point with g' , $f^{g'g}$ the contact force that g' exerts on g , and A^g is the area enclosed by the cell centers and contact points surrounding disc g , as illustrated in Fig. 1. The cell stress σ^c is then

$$\sigma^c = \sum_{g \in c} A^g \sigma^g / \sum_{g \in c} A^g, \quad (4)$$

with $g \in c$ denoting the discs surrounding cell c .

A cell order is the number of discs surrounding it.

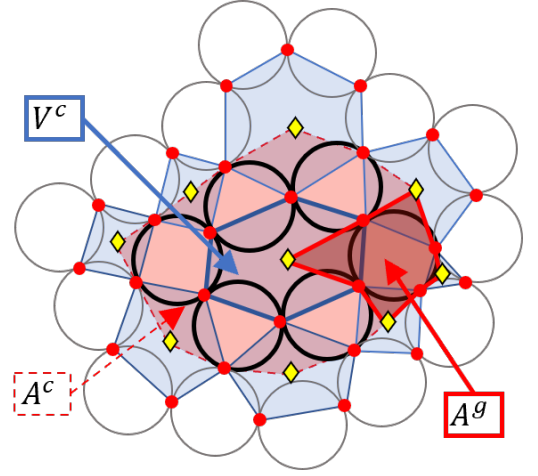


FIG. 1. Cell definition and structure. Central blue polygon: the cell [3, 4, 9] of area V^c , surrounded by the discs shown in thick black lines; red points: contacts; yellow diamonds: cell centers, defined as the mean positions of the contacts surrounding a cell; dark red polygon: the area associated with a disc, A^g , used to calculate the disc stress; dashed red polygon: the sum over the disc areas A^g around the cell, A^c , used to calculate the cell stress.

The static and dynamic cell order distribution (COD), $Q(n)$, were shown to have remarkable properties: maximum entropy [15], detailed balance [12, 17], and forming a basis to determining the random close packing [18]. Our measured CODs agree well with those reported in [3, 4] and they are not exponential as in [15, 18]. This is because the COD is governed by a competition between mechanical stability and entropy maximisation [15], with the latter dominant only when the external confining and driving forces are low. This condition is not satisfied in our compression processes.

Another reported feature of the COD is that the orders of neighbor cells are uncorrelated [12, 17]. Our findings support those observations and show, furthermore, that this feature is independent of the process. Nevertheless,

systems with different values of μ collapse to different curves. This is illustrated in Fig. 2 for the PDFs of n around a cell of order n' , $Q(n|n')$ $\mu = 0.01$ and 10.0 . The PDFs for the scaled variable $x \equiv (n-2)/n-2$ are fitted well by a $k - \Gamma$ distribution

$$P(x) = \frac{k(\mu)^{k(\mu)} x^{k(\mu)-1}}{\Gamma[k(\mu)]} e^{-k(\mu)x}, \quad (5)$$

with $k(\mu)$ decreasing monotonically from 4.2 ± 0.5 at $\mu = 0.01$ to 2.9 ± 0.3 at $\mu = 10.0$ (See Fig. 5 in the supplemental material (SM) [19]). Typical collapsed curves and their fits are shown in Fig. 2 for $\mu = 0.01$ and 10.0 .

Turning to cell stresses, the principal stresses are σ_1^c

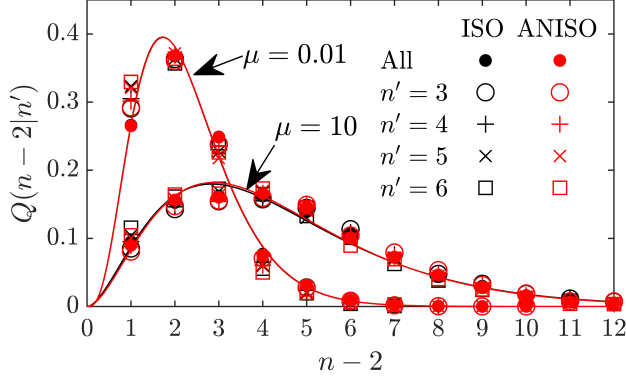


FIG. 2. The conditional cell order distributions, $Q(n|n')$, of all the systems and all cell orders, n' , collapse onto a single curve that depends only on μ . Shown are the collapsed curves for $\mu = 0.01$ and $\mu = 10.0$. The solid lines represent $k - \Gamma$ -distribution fits, eq. (5).

and $\sigma_2^c < \sigma_1^c$, the mean and deviatoric cell stresses are, respectively, $p = (\sigma_1^c + \sigma_2^c)/2$ and $q = (\sigma_1^c - \sigma_2^c)/2$. We expect cell stability to be sensitive to the ratio $h = q/p$, which is supported by our model below. The PDFs of h are found to be also independent of the packing process. With increasing μ , they get broader and their mean, \bar{h} , increases (Fig. 6 in the SM [19]).

To understand the PDF of h , we decompose it to its conditional probabilities in n -disc cells, $P(h|n)$:

$$P(h) = \sum_n Q(n) P(h|n), \quad (6)$$

where $Q(n)$ is the fraction of cells of order n . The mean at order n , $\bar{h}(n) = \sum_n h P(h|n)$, decreases with n at roughly the same rate in all the systems, $\partial \bar{h}(n)/\partial n = -0.015 \pm 0.001$ (see the SM [19]). Thus, cell stability to deviatoric stress decreases with increasing cell order, consistent with the conclusions in [4] and [15]. We also see that $\partial \bar{h}(n)/\partial \mu > 0$, evidence for friction increasing cell stability.

Rewriting (6) as

$$P(h) = \sum_n Q(n) P(\hat{h}(n)|n)/\bar{h}(n), \quad (7)$$

we find that, remarkably, all the PDFs $P(\hat{h}|n)$ collapse onto one curve, shown in Fig. 3, independent of n , μ , and compression process. This curve is fitted well by a single Weibull PDF:

$$P\left(\hat{h}(n)|n \equiv \frac{h(n)}{\bar{h}(n)}|n\right) = \frac{m}{\lambda} \left(\frac{\hat{h}(n)}{\lambda}\right)^{m-1} e^{-(\hat{h}(n)/\lambda)^m}, \quad (8)$$

with $\lambda = 1.128 \pm 0.006$ and $m = 2.09 \pm 0.015$. Of these parameters one is independent and the other determined by normalization. Checking the global PDF, $P(\hat{h} \equiv \frac{h}{\bar{h}})$, we find that the PDFs of all the systems indeed collapse onto the same functional form (Fig. 7 in the SM [19]). These collapses are indicative of an underlying self-organization and universality [3, 4] and we study in further detail next.

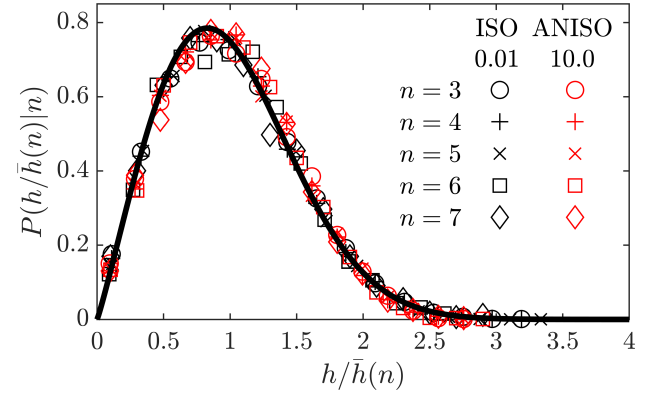


FIG. 3. The conditional PDFs of \hat{h} given n , when normalized by the mean $\bar{h}(n)$, collapse onto a single curve for all cell orders and friction coefficients. The solid line represents Weibull-distribution fit, eq. (8).

Stress-structure self-organization

The above collapses show self-organisation of the stress with the cell order and, to establish stress-structure co-organization, we next look into the local relations between the two. The cell configurations determines the local structure and it has been demonstrated that the co-organization is affected directly by the competition between maximizing configuration multiplicity and mechanical stability [4, 15]. To quantify the stress-structure relation, we first approximated each cell by its best fitted ellipse, using the method detailed in the SM [19]. We then studied the correlation between the cell orientation, defined as the direction of its ellipse's major axis, θ^c , and the principal cell stress direction, θ^σ . The orientations of θ^σ and θ^c follow the boundary stresses, which are not uniform in ANISO (see Fig. 4 in the SM [19]). To eliminate the boundary effect, we computed for each cell order the normalized joint PDFs $\frac{P(\theta^c, \theta^\sigma|n)}{P(\theta^c|n)P(\theta^\sigma|n)}$, plotted in Fig. 4 for ISO packings. The plots show a strong correlation between the cell orien-

tations and stress principal in all the systems, except for cells of order 3, whose stability allows large orientational deviations from their stress principal axes and whose orientations are not well-characterized.

It is important to note that, while the peaks in these

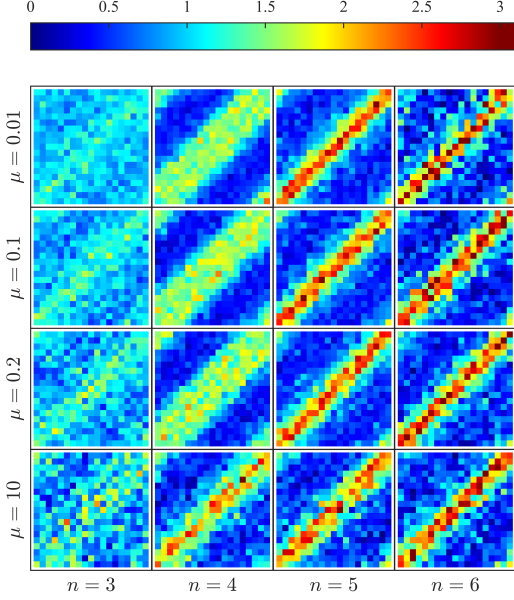


FIG. 4. The conditional joint PDF of θ^σ and θ^c for cell orders $3 \leq n \leq 6$ in ISO systems exhibit a clear peak at $\theta^\sigma = \theta^c$.

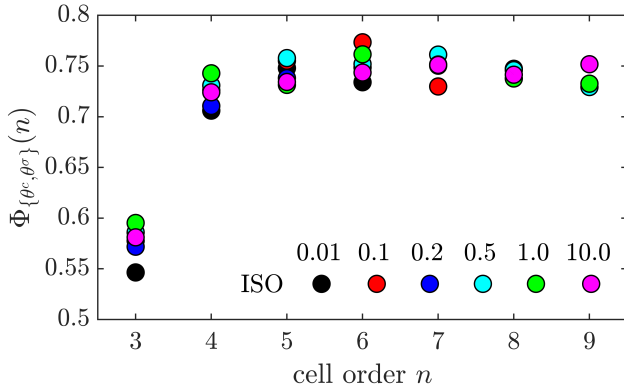


FIG. 5. The correlation coefficients between θ^σ and θ^c given cell order n , $\Phi_{\{\theta^c, \theta^\sigma\}}(n)$, against n .

plots get sharper as n increases, the plots are hardly affected by μ . The plots for ANISO packings, shown in the SM [19], exhibit identical behavior. Thus, cell stability and shapes appear independent of friction, suggesting that common wisdom concerning the effect of friction on these characteristics should be reconsidered. We also show in the SM [19] the unconditional joint PDF, $\frac{P(\theta^c, \theta^\sigma)}{P(\theta^c)P(\theta^\sigma)}$, which behaves similarly.

To quantify the stress-structure correlation, we com-

puted the correlation coefficient between θ^c and θ^σ for each order,

$$\Phi_{\{\theta^c, \theta^\sigma\}}(n) = \frac{\sum_{i \in n} \delta\theta_i^c \delta\theta_i^\sigma}{\left[\sum_{i \in n} (\delta\theta_i^c)^2 \sum_{j \in n} (\delta\theta_j^\sigma)^2 \right]^{1/2}}, \quad (9)$$

where $\delta\theta_i^c$ and $\delta\theta_i^\sigma$ are the differences from the respective mean angles at a given n . Fig. 5 shows that the correlation is roughly the same for all systems, $\Phi = 0.73 \pm 0.03$, except for 3-disc cells, $\Phi = 0.57 \pm 0.02$, for the reasons discussed above.

A model for the stress-structure organization

To understand the cooperative alignment of cells with the local principal stress, we model a cell by its equivalent ellipse, whose major axis is tilted by an angle $\Delta\theta = \theta^\sigma - \theta^c$ relative to the local principal stresses (Fig. 6). In the cell's frame of reference, the stress is

$$\Sigma = \begin{bmatrix} \sigma_1 + \sigma_2 \tan^2 \Delta\theta & 2q \tan \Delta\theta \\ 2q \tan \Delta\theta & \sigma_1 \tan^2 \Delta\theta + \sigma_2 \end{bmatrix} \cos^2 \Delta\theta \quad (10)$$

This generates a torque on the cell, whose stability de-

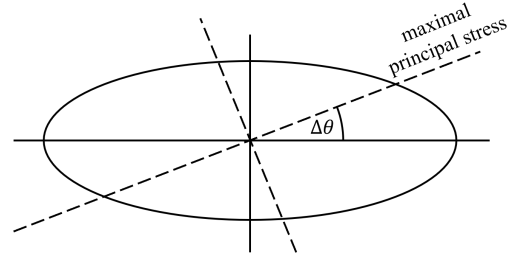


FIG. 6. When the local stress principal axes (dashed lines) are tilted relative to the cell's equivalent ellipse by an angle of $\Delta\theta = \theta^\sigma - \theta^c$, there is a torque moment on the cell.

pends on the magnitude of the ratio of the shear stress, $\tau = 2q \sin \Delta\theta \cos \Delta\theta$, to the mean cell stress, p ,

$$\frac{\tau}{p} = h \sin(2\Delta\theta). \quad (11)$$

For a given friction, the larger the curvature along the cell circumference the smaller the tangential-to-normal force ratio at a contact between particles and the less likely is the contact to slide and fail. Aligning then the maximal principal stress with the highest ellipse curvature leads directly to the conclusion that the smaller the angle $\Delta\theta$ the more stable the cell. This model is validated against the data, as shown in Fig. 7. Each red point in this plot represents a cell with specific h and the ratio τ/p . The data is clustered at low $\Delta\theta$ for any value of h (black line contours), indicating the higher stability of cells with low torque moments.

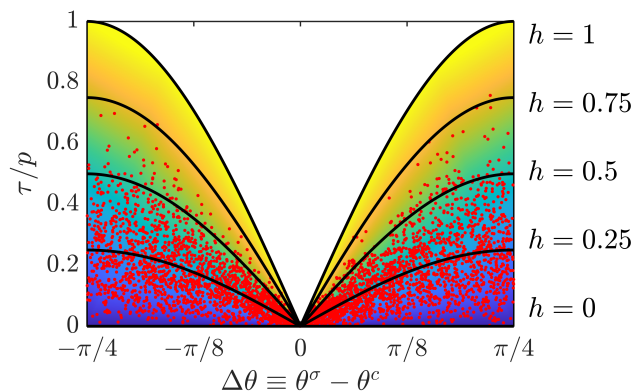


FIG. 7. A scatter plot of cells in the $\Delta\theta - \frac{\tau}{p}$ parameter space. Each red point represents a cell and the background colour represents increasing value of h from blue ($h = 0$) to yellow ($h = 1$). The black lines are contours of constant h . The increasing cell density with low values h and $\Delta\theta$ support the model that cell-stress alignment is governed by stability against local torque moment.

Conclusions

To conclude, we simulated isotropic (ISO) and anisotropic (ANISO) compressions of two-dimensional disc systems of interparticle friction coefficients, $0.01 \leq \mu \leq 10.0$, to study and quantify the local relation between stress and structure during their self-organization. The local structure was characterized through the cell orders and orientation and cell stresses were defined. We have reported the following. 1. The PDFs of the cell stress ratios at each order n , $h(n) = (\sigma_1^c - \sigma_2^c)/(\sigma_1^c + \sigma_2^c)$, scaled by their means, $\bar{h}(n)$, collapse onto a single curve that is independent of n , μ , and packing process. This curve is fitted well by a Weibull PDF. The cell stress ratios of all the cells, scaled by the mean stress ratio collapses onto one curve. 2. The mean stress ratio at cell order n , decreases with n and increases with μ , independently of the packing process. 3. The cell orientations, quantified by the directions of the major axes of their equivalent ellipses, clearly align along the major principal cell stress directions. 4. Excepting the relatively rounded 3-disc cells, the cells stress-orientation correlation is roughly independent of n , μ , and packing process. 5. A first-principles model was constructed, which shows that the correlation in 4 is governed by cell stability to contact sliding.

These results have several important implications. The overall collapse of the PDFs of \hat{h} for all n to a Weibull PDF form is yet unexplained, but this observation should encourage a search for a fundamental model to derive it. A similar PDF governs threshold stresses for opening of microcracks and an analogy between contact breaking and microcrack opening might lead to such a model.

The strong local correlation between cell and stress orientations is direct evidence for the cooperative stress-structure self-organization on the particle scale during quasistatic dynamics and this correlation.

Significantly, this calls into question continuum linear stress field theories for granular media, which assume independence of the medium's constitutive properties of the stress. Our results show clearly that, on applying boundary stress, the local structure re-organizes, which must modify the local constitutive properties. The dependence of the constitutive properties on the local stress makes the stress field equations nonlinear [2], suggesting that a new theory, based on local micromechanics, is required for describing stress transmission in granular media.

RB acknowledges the financial support of the JSPS Invitational Fellowship ID=S22039 and the hospitality of Tsukuba University. TM acknowledges the financial support of JSPS KAKENHI Grants 20K20434A, 21H01422, and 21KK0071.

* jiang.xiaoyu.fp@u.tsukuba.ac.jp

† tmatsu@kz.tsukuba.ac.jp

‡ rbb11@cam.ac.uk

- [1] A. Tordesillas, and M. Maya. On the modeling of confined buckling of force chains. *J. Mech. Phys. Solids* **57**, 707 (2009).
- [2] R. Blumenfeld, S. F. Edwards, and S. M. Walley, Granular systems, in *The Oxford Handbook of Soft Condensed Matter*, edited by E. M. Terentjev and D. A. Weitz (Oxford University Press, Oxford, 2015) Chap. 5.
- [3] T. Matsushima and R. Blumenfeld, Universal structural characteristics of planar granular packs, *Phys. Rev. Lett.* **112**, 098003 (2014).
- [4] T. Matsushima and R. Blumenfeld, Fundamental structural characteristics of planar granular assemblies: Self-organization and scaling away friction and initial state, *Phys. Rev. E* **95**, 032905 (2017).
- [5] T. Matsushima and R. Blumenfeld, Statistical properties of cell stresses in 2D granular solids, *EPJ Web Conf.* **249**, 02006 (2021).
- [6] M. Oda, S. Nemat-Nasser, and J. Konishi, Stress-induced anisotropy in granular masses, *Soils Found.* **25**, 85 (1985).
- [7] R. P. Seelig and J. Wulff, The pressing operation in the fabrication of articles by powder metallurgy, *POWDER METALL, UK* **166**, 492 (1946).
- [8] M. Cates, J. Wittmer, J.-P. Bouchaud, and P. Claudin, Jamming, force chains, and fragile matter, *Phys. Rev. Lett.* **81**, 1841 (1998).
- [9] R. C. Ball and R. Blumenfeld, Stress field in granular systems: loop forces and potential formulation, *Phys. Rev. Lett.* **88**, 115505 (2002).
- [10] A. Donev, R. Connelly, F. H. Stillinger, and S. Torquato, Underconstrained jammed packings of non-spherical hard particles: ellipses and ellipsoids, *Phys. Rev. E* **75**, 051304 (2007).

- [11] N. P. Kruyt and L. Rothenburg, A micromechanical study of dilatancy of granular materials, *J. Mech. Phys. Solids* **95**, 411 (2016).
- [12] C. C. Wanjura, P. Gago, T. Matsushima, and R. Blumenfeld, Structural evolution of granular systems: theory, *Granular Matter* **22**, 1 (2020).
- [13] A. Tordesillas, D. M. Walker, and Q. Lin, Force cycles and force chains, *Phys. Rev. E* **81**, 011302 (2010).
- [14] M. R. Kuhn, Dense granular flow at the critical state: maximum entropy and topological disorder, *Granular Matter* **16**, 499 (2014).
- [15] X. Sun, W. Kob, R. Blumenfeld, H. Tong, Y. Wang, and J. Zhang, Friction-controlled entropy-stability competition in granular systems, *Phys. Rev. Lett.* **125**, 268005 (2020).
- [16] P. Cundall and O. Strack, A discrete numerical model for granular assemblies, *Géotechnique* **29**, 47 (1979).
- [17] X. Sun, Y. Wang, Y. Wang, R. Blumenfeld, and J. Zhang, Experimental evidence of detailed balance in granular systems, arXiv preprint arXiv:2105.01355 (2021).
- [18] R. Blumenfeld, Disorder criterion and explicit solution for the disc random packing problem, *Phys. Rev. Lett.* **127**, 118002 (2021).
- [19] See Supplemental Material at [URL] for more relevant results.

Coordinated Stress-Structure Self-Organization in Granular Packing

Supplemental material

(Dated: August 16, 2022)

A. The area associated with a disc

The hatched area, shown in Fig. 1, is the area associated with disc g , A^g . This area is used to normalize the force moment tensor for obtaining the disc's stress tensor.

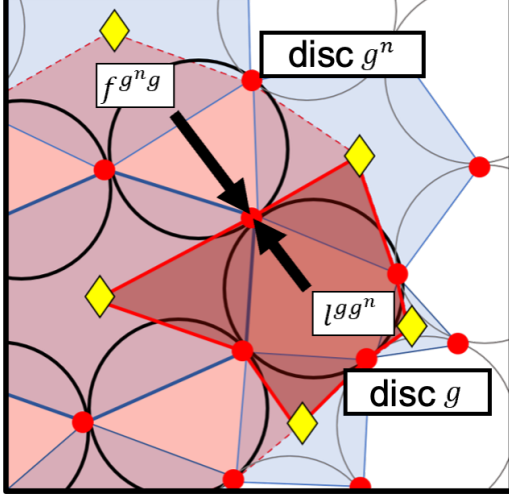


FIG. 1. Zoom-in view of the area associated with disc g , A^g . Shown by thick black arrows are the force that disc g^n exerts on disc g and the position vector of the contact, where it is applied.

B. The steady decrease of $\bar{h}(n)$ with n

The mean stress ratio of cells of order n , $\bar{h}(n)$, decreases as n increases. This is evidence that cells become increasingly unstable with their order. Specifically, the high-order cells can support a smaller difference between the principal stresses than low-order cells.

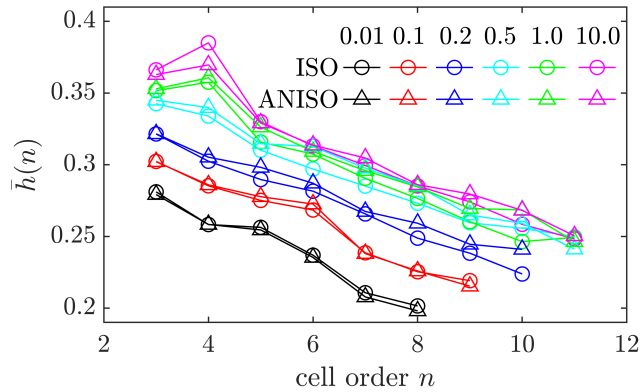


FIG. 2. The steady decrease of the mean stress ratio, $\bar{h}(n)$, with cell order. The decrease rate appears independent of both friction and compression protocol.

C. The approximation of cell shape as an ellipse

The description of the polygonal cell as its best-fitted ellipse is done as follows. The general ellipse equation is

$$Ax^2 + Bxy + Cy^2 + Dx + Ey + F = 0. \quad (1)$$

Note that, for our purposes, the value of F is irrelevant because we are interested only in the ellipse orientation. To use the least squares method, we define a column vector $P = (A, B, C, D, E)$ of the parameters to be fitted. The computational cost per cell node, $\mathcal{C}(P)$, is the square of the left hand side of (1). The computational cost for m nodes, (x_i, y_i) , $i = 1, 2, \dots, m$ can be presented in a matrix form,

$$\begin{aligned} \mathcal{C}(P) &= (XP + f)'(XP + f) \\ &= P'X'XP + 2f'XP + f^2, \end{aligned} \quad (2)$$

in which f is a column vector composed of m elements of F , and

$$X = \begin{pmatrix} x_1^2 & x_1y_1 & y_1^2 & x_1 & y_1 \\ x_2^2 & x_2y_2 & y_2^2 & x_2 & y_2 \\ \vdots & \vdots & \vdots & \vdots & \vdots \\ x_m^2 & x_my_m & y_m^2 & x_m & y_m \end{pmatrix}. \quad (3)$$

Taking the derivative of $\mathcal{C}(P)$ with respect to the parameter vector P , yields

$$P'X'X = -f'X = -FY, \quad (4)$$

in which Y is a five-elements column vector. The i th element is the sum over the i th column of X . Dividing both sides by the irrelevant parameter $-F$, we have $P'_0X'X = Y$, and the parameter vector $P_0 = (A_0, B_0, C_0, D_0, E_0)$ can be solved by Gauss elimination. An illustration of the results of this method is shown in Fig. 3.

The cell orientation θ^c , is found from P_0 :

$$\theta^c = \frac{1}{2} \arctan \frac{B_0}{C_0 - A_0}. \quad (5)$$

For calculation of other ellipse parameters, such as the center position, size, perimeter, etc., see documentation at: https://www.mathworks.com/matlabcentral/fileexchange/3215-fit_ellipse.

Since one requires at least five vertices to estimate the five parameters, it is necessary to add nodes cells of orders 3 and 4. To this end we use for these cells both the contact points and the disc centers (red circles and dark squares in Fig. 3, respectively). This yields six

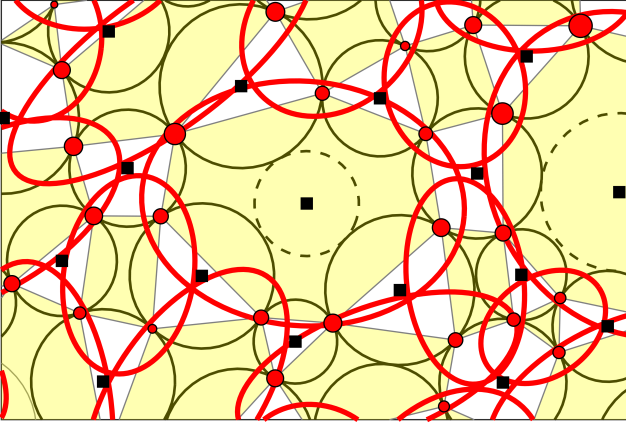


FIG. 3. The best-fitted ellipses for several cells are shown by red lines. Small red circles represent the contact points and dark squares represent disc centers.

and eight nodes for cells of orders 3 and 4, respectively.

D. The spatial uniformity of the cell stresses

The isotropic compression in the ISO systems is expected to yield an internal uniform distribution of cell orientations and large principal stresses, which is exactly what is observed in Fig. 4 (circular symbols). However, the nonuniform boundary stresses in the anisotropic compression procedure, ANISO, is expected to give rise to distributions of these quantities that peak and dip at $\pm\pi/2$ and 0, respectively. This is indeed what we observe, as shown in Fig. 4 (triangular symbols).

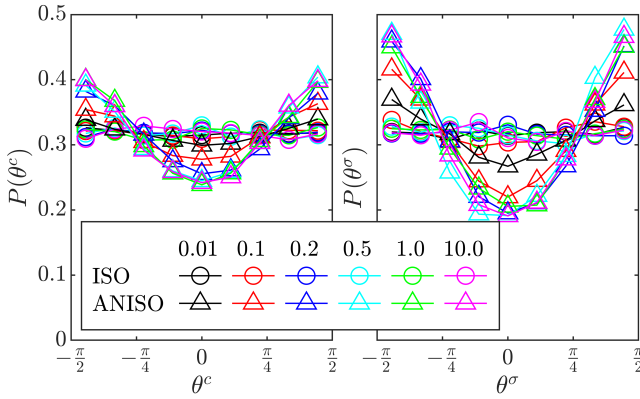


FIG. 4. The distributions of the cell orientations, θ^c (left), and principal cell stresses, θ^σ (right), relative to the boundary for all systems.

E. The dependence of $Q(x|n')$ on μ

The conditional PDFs $Q(x|n')$, where $x = (n-2)/(n-2)$, is a measure of the COD around n' for a system of interparticle friction μ . These PDFs are shown in the main text to collapse onto the same curve for all n' and

regardless of whether the process is ISO or ANISO. The collapsed curves are fitted well by a $k - \Gamma$ distribution

$$P(x) = \frac{k(\mu)^{k(\mu)} x^{k(\mu)-1}}{\Gamma[k(\mu)]} e^{-k(\mu)x}, \quad (6)$$

with k depending only on μ and decreasing monotonically from 4.2 ± 0.5 at $\mu = 0.01$ to 2.9 ± 0.3 at $\mu = 10.0$, as shown in Fig. 5.

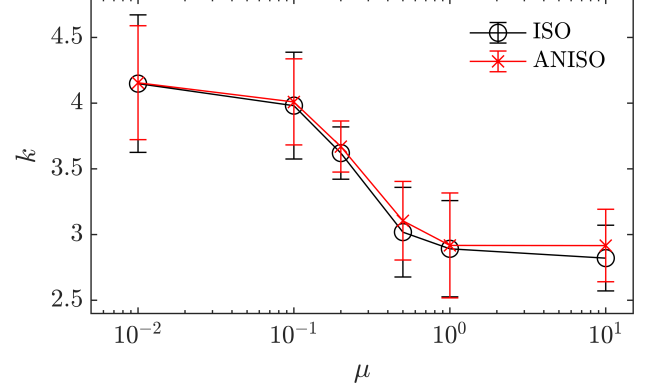


FIG. 5. The dependence of the fitting parameter k on the intergranular friction coefficient μ .

F. The PDFs of the cell stress ratios

In Fig. 6 below, we display the raw PDFs of the cell stress ratios, $h = q/p$, for all the cell orders, given the friction coefficient. These coefficients are detailed as a legend in the figure. As shown in the main text, all these PDFs collapse onto a single curve when normalised by the mean stress ratio, \bar{h} , which also depends on n . Scal-

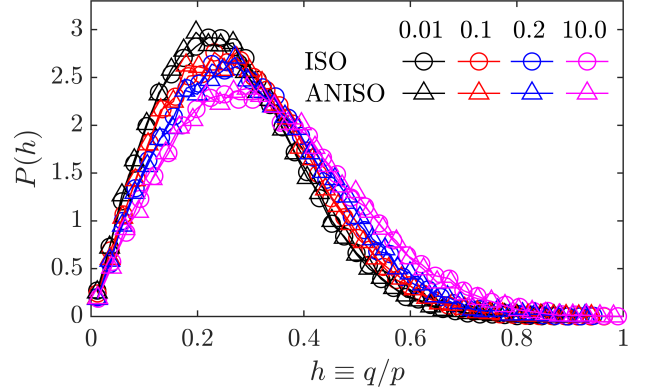


FIG. 6. The PDF of the cell stress ratio, $h = q/p$

ing by the mean, the PDFs of $\hat{h} \equiv h/\bar{h}$ collapse onto a single curve for all systems and all values of μ , as shown in Fig. 7, albeit with small fluctuations near the peak. The collapsed curve is fitted well by the single Weibull PDF discussed in the main text.

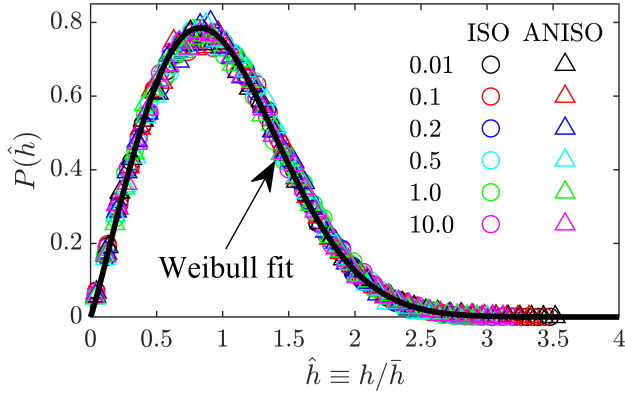


FIG. 7. The PDFs of $\hat{h} \equiv h/\bar{h}$ collapse onto a single curve, fitted excellently by a Weibull PDF (solid line).

G. The normalised joint PDF, $P(\theta^c, \theta^\sigma)$

In Fig. 8, we display the normalized joint PDFs of the orientations of the cell stresses and cell ellipses. The plotted PDFs are normalized as

$$\frac{P(\theta^c, \theta^\sigma)}{P(\theta^c)P(\theta^\sigma)} \quad (7)$$

to eliminate non-uniform effects caused by the boundary stresses (see discussion in the main text).

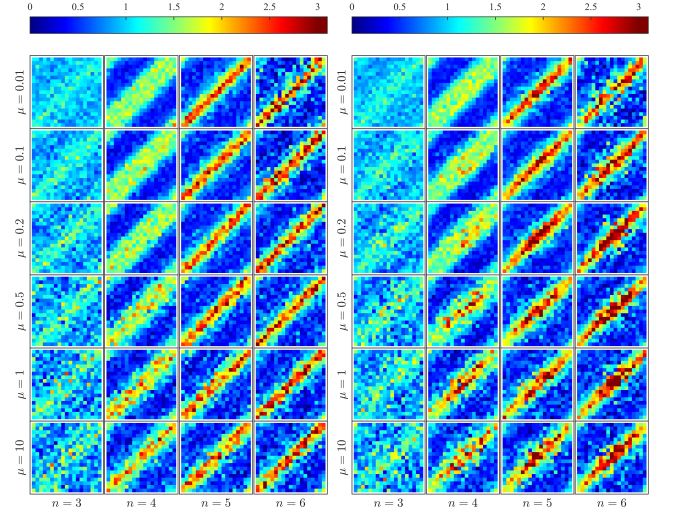


FIG. 8. The joint PDF of θ^σ and θ^c , scaled using eq. (7), plotted in the $\theta^c - \theta^\sigma$ plane: a) for all the isotropically compressed systems; b) for all the anisotropically compressed systems. In all the plots, $-\pi/2 < \theta^c, \theta^\sigma \leq \pi/2$.